

# WISE photometry of EXor sources and candidates

S.Antoniucci<sup>a</sup>, T.Giannini<sup>a</sup>, D.Lorenzetti<sup>a,\*</sup>

<sup>a</sup>*INAF - Osservatorio Astronomico di Roma - Via Frascati, 33 - 00040 Monte Porzio Catone, Italy*

---

## Abstract

We present a collection of *WISE* photometry of EXor sources and candidates (more recently identified). This represents the first complete survey of such objects in the mid-IR (3.4 - 22  $\mu$ m) that was carried out with the same instrumentation. Two-color diagrams constructed with *WISE* data evidence a clear segregation between classical and newly identified sources, being these latter characterized by colder (and less evolved) circumstellar disks. By combining 2MASS and *WISE* data, we obtain spectral energy distributions (SED's) that are compatible with the existence of an inner hole in the circumstellar disk. A compilation of all EXor observations given in the literature at wavelengths very similar to those of *WISE* is also provided. This allows us to study their mid-IR variability, which has been poorly investigated so far and without any coordination with shorter wavelengths surveys. The presented *WISE* photometry and the compilation of the literature data are intended as a first step toward the construction of a significant database in this spectral regime. Preliminary indications on the mechanisms responsible for the luminosity fluctuations are provided.

*Key words:* Stars: pre-main sequence, variable, infrared: stars, Astronomical Data Bases: catalogs

---

## 1 Introduction

Two decades ago a new class of young stellar objects (YSO's) was defined and studied by Herbig (1989, 2008), who dubbed them as EXor sources, after the

---

\* Corresponding author.

*Email addresses:* `simone.antoniucci@oa-roma.inaf.it` (S.Antoniucci),  
`teresa.giannini@oa-roma.inaf.it` (T.Giannini),  
`dario.lorenzetti@oa-roma.inaf.it` (D.Lorenzetti).

name of the prototype EX Lup. These pre-Main Sequence stars are characterized by repetitive outbursts in optical light of amplitudes up to 4-5 mag. Such outbursts typically last one year or less and are followed by long-lasting (5-10 yr) quiescence periods. They are due to intermittent accretion events during which the matter accumulated in the inner parts of the circumstellar disks is violently transferred onto the central star inducing a shock on its surface, whose cooling determines an impulsive increase of its luminosity. The physical mechanism and the observational appearance of the EXor events make these objects substantially similar to FUors (Hartmann & Kenyon 1985), although these latter present outbursts of larger intensity and remain in that state for longer period (tens of years).

So far, about 20 EXor systems are known, which can be grouped into two sub-classes: the classical EXor (Herbig 1989, 2008), and the newest identifications (listed in Lorenzetti et al. 2012a). Historically, the first group was identified in the visual band, which means that these accretion-disk systems are essentially unobscured (i.e. without significant envelopes). Later on, the increasing availability of near-IR facilities quite naturally favoured the identification of more embedded eruptive variables (second sub-class), typically associated with an optical-IR nebula. The membership to this latter class often relies on the detection of sporadic outbursts and does not stem from a more comprehensive analysis aimed at checking all the properties typical of the classical prototypes (i.e. repetitive outbursts, rapid brightening and slower fading, colors pre-and post-outburst). The similarities and differences between the classes are discussed in more detail in Lorenzetti et al. (2012a). Here we recall that the newest ones are in general more embedded objects whose phenomenology is typically observed at infrared (IR) (1-10  $\mu\text{m}$ ) wavelengths. Indeed, given the mechanism that originates the outburst, there is no reason preventing the intermittent accretion from occurring also during a more embedded phase. To study the modalities of the EXor brightness fluctuations, we are conducting since a few years a photometric (Lorenzetti et al. 2007) and spectroscopic (Lorenzetti et al. 2009, 2012b) monitoring of EXors in the near-IR. Of particular interest is the mid-IR domain (3-25  $\mu\text{m}$ ), where many EXors emit most of their energy. The spectral behaviour at these wavelengths is strictly related to disk and envelope regions located at radial distances (from the central star) where disk fragmentation and planet formation occur. The difficult access to facilities operating in this spectral range has hampered this kind of studies, apart from few important exceptions (Kóspál et al. 2012 and references therein). However, during the last years IR surveys (e.g. *MSX*, *Spitzer*, *AKARI*) allowed the investigation of entire samples of sources at mid-IR frequencies. Very recently, the satellite *WISE* (Wright et al. 2010) has covered the whole sky at 3.4, 4.6, 12, and 22  $\mu\text{m}$ , and we present here the *WISE* photometry of the EXors aiming at: (i) building up the first mid-IR catalog of these objects, which would serve as a reference for future and past (unfortunately very few and sparse) observations; (ii) providing a

complete database for constructing spectral energy distributions; *(iii)* fostering the study of the EXor variability in this still unexplored spectral range, practically unaffected by extinction. The paper is organized in the following way: in Sect.2 we introduce the investigated EXors providing their *WISE* photometry, which is then discussed in Sect.3. In Sect.4 a database of the mid-IR observations collected so far in photometric band-passes very similar to those of *WISE* is given along with a short discussion on the detected variability cases. Finally, our concluding remarks are presented in Sect.5.

## 2 Our sample and *WISE* photometry

The sample we consider in the present paper is composed of the classical and newest EXors, which are listed in the upper and lower part of Table 1, respectively. The *WISE* photometry of the sources is given (columns 2 to 9) in terms of magnitudes and relative errors. The physical parameters of all these objects (with the corresponding references) can be found in Table 1 of Lorenzetti et al. 2012a.

As described by Cutri et al. 2012, all magnitudes listed in the *WISE* Source Catalog have been photometrically calibrated using observations of a network of standard stars that are located near the ecliptic polar caps. In that paper, the process by which instrumental source magnitudes were converted to calibrated magnitudes is also described. All the sources listed in Table 1 present a photometric quality flag AAAA, which means that the source is detected in all 4 bands with a signal-to-noise ratio  $> 10$ . Saturation begins to affect sources brighter than approximately 8.1, 6.7, 3.8, and -0.4 mag at 3.4, 4.6, 12, and 22  $\mu\text{m}$ , respectively. *WISE* profile-fit photometry of saturated sources is obtained by fitting the Point Spread Function (PSF) to the non-saturated pixels in the profile wings. The accuracy of photometric measurements of saturated sources degrades with increasing brightness. For our sources, however, saturation typically affects less than 30% of the pixels, hence this effect does not alter our conclusions, as discussed below in the specific sections. Column 9 gives the variability flag, whose definition and significance is discussed in the next paragraph. As additional information, columns 10 and 11 of Table 1 report the distance (in arcsec) between the positions of the *WISE* source and associated 2MASS PSC object and the Position Angle (in degrees from N to E) of the relative separation vector. In the large majority of cases (14 out of 18) such distance is  $\lesssim 1$  arcsec, which proves that 2MASS and *WISE* are almost certainly looking at the same source.

*WISE* also provides a record of multi-epoch (on a daily time-scale) measurements from the individual images that were co-added to extract the Catalog fluxes given in Table 1. Typically, a dozen of independent exposures were

acquired for each point near the ecliptic so that these multiple observations could be fruitfully investigated to look for clues of short time-scale variability. The *WISE* Catalog entries include a variability flag (see Table 1 - col.9) consisting of a four-character string (one character per band) giving a measure of the probability that the source is variable in each band. The derivation of this flag is discussed by Cutri et al. 2012 and by Hoffman et al. 2012; both descriptions emphasize the need to exclude *WISE* single-exposure measurements that *i*) come from low quality images, *ii*) are saturated, *iii*) have large reduced  $\chi^2$  values in profile fitting, plus other reasons. Hence, indication of variability from the Single-exposure Catalog can be conservatively taken into account only for those bands that present a variability flag value  $\gtrsim 7$  (see Table 1 caption). In our case, eight sources (namely VY Tau, DR Tau, V1118 Ori, NY Ori, LDN1415 IRS, V2775 Ori, V2492 Cyg, and V2493 Cyg) have a high probability of presenting short-time variability in one or more bands. In the following we will cautiously use these data as a further support to cases of (independently ascertained) daily variability. Finally, another *WISE* database is in principle available for studying the variability of the objects, namely the preliminary release of Post-Cryogenic data. However, some caution should be exercised when comparing cryo and post-cryo photometry, because there is only a preliminary calibration available at the moment. For this reason we decided not to include these data in the present paper.

### 3 Results and discussion

#### 3.1 *WISE* color diagrams

The *WISE* photometry given in Table 1 is presented in Figure 1 in form of two color plots [3.4-4.6] vs. [4.6-12] (lower panel) and [4.6-12] vs. [12-22] (upper panel). Possible saturation (only for the brightest objects) marginally affects the *WISE* photometry in the four bands, thus its effect on colors is expected to be negligible. EXors are located in loci framed by a color dispersion  $\gtrsim 2$  mag: between 0.4 and 3 mag for the [3.4-4.6] color and between 1 and 3 mag for all the other colors. Expectedly, these are the loci typically pertaining to the pre-Main Sequence objects characterized by a significant level of IR excess over the photospheric continuum. Classical (newest) EXors are represented in Figure 1 with blue open (red solid) symbols, respectively. A segregation between the two sub-classes is noticeable in all the colors, being the newest also the reddest objects. Particularly evident is the segregation in the [3.4-4.6] color, which is  $> 1$  for the newest and  $< 1$  for the classical EXors, the unity value corresponding to a ratio  $F_\nu(3.4\mu\text{m})/F_\nu(4.6\mu\text{m}) \approx 4$ . Although classical objects are certainly less obscured than the newest ones, the color separation between the two classes is certainly due also to intrinsic effects.

Indeed, it is impossible to superpose newest EXors to the classical ones, not even considering a differential extinction larger than 10 mag (arrows depicted in Figure 1). Hence, the SED's of sources of the two sub-classes should be intrinsically different (see Sect.3.2). From Figure 1 it is also evident that the *WISE* colors of EXor objects are not consistent with a single black-body, but can be reproduced considering different dust components with the highest temperature ranging between 1000 and 3000 K and the lowest one between 380 and 500 K. Oversimplifying, in Figure 1 we depict only pairs of black-body functions, but a more realistic stratification of temperatures should be envisaged.

### 3.2 EXor near- and mid-IR SED's

We obtained the near- and mid-IR SED's of EXors by identifying the counterparts at shorter wavelengths (JHK bands) of the sources listed in Table 1. Unfortunately, a single epoch SED cannot be constructed since coordinated observations in different spectral ranges are very rare (see Sect. 4). However, to rely on a data-base as uniform as possible, we considered the 2MASS (Struck et al. 2006) counterparts that match our sources within 2 arcsec or less (see Table 1). All the listed EXors (except one, V2492 Cyg) have been associated to a 2MASS counterpart and the resulting SED's are depicted in Figures 2 and 3. For comparison, a median stellar photosphere in the spectral range K5-M5 is also plotted in each panel (Hernández et al. 2007), normalized to the J-band flux of the source. As anticipated by the two-color diagrams, also the SED shapes of the two sub-classes are substantially different. Emission from all the classical EXors (except for NY Ori) declines with increasing wavelength for  $\lambda \lesssim 10 \mu\text{m}$ ; at  $\lambda \gtrsim 10 \mu\text{m}$  their SED's tend to increase, showing an excess more pronounced than that at shorter wavelengths. Conversely, the newest candidates (apart from two exceptions) have SED's that monotonically increase with wavelength. The spectral distributions of both classes are fully consistent with those predicted by D'Alessio et al. (1999), namely they originate from a temperature stratification related to a more (classical EXor) or less (newest ones) evolved circumstellar disk. To give a quantitative evaluation of the EXor SED's we introduce as empirical indicator the parameter  $\varepsilon$ , i.e. the ratio of the total 1-22  $\mu\text{m}$  luminosity to the luminosity of a median K5-M5 photosphere. In this first-order approximation the J-band flux is assumed to be entirely photospheric, as implied by the normalization used to show the SED's in Figures 2 and 3. The obtained values of  $\varepsilon$  are given in the last column of Table 1: the relatively modest excess presented by the classical EXors is accounted for by their  $\varepsilon$  values  $\lesssim 20$ , while the newest ones present  $\varepsilon$  typically  $\gg 200$ , except for the two unobscured T Tauri stars V2492 and V2493 Cyg. This short analysis evidences how the mid-IR emission is crucial for observationally defining the EXor class of objects. Finally, and more spec-

ulatively, we can observe that the majority of EXor SED's (10 out of the 16 depicted in Figures 2 and 3) seem to show a deficit of emission around  $3\ \mu\text{m}$ . This appearance should be considered very cautiously since that wavelength is exactly the matching point between 2MASS and *WISE* photometry, and 2MASS data were obtained about ten years before the *WISE* advent. On the other hand, a systematic trend according to which *WISE* data would have been taken when all the sources were in a stage more quiescent than 2MASS, sounds remarkably strange. Saturation could cause the aperture photometry to be systematically underestimated, so that, accounting for this effect, the observed deficit could be partially reduced in DR Tau and V512 Per. However, the same effect would definitely enhance the discontinuity in NY Ori, V1647 Ori, and V2775 Ori. In any case, if such an emission deficit will be confirmed by forthcoming observations, it reasonably indicates a lack of emission in that spectral range, which is usually interpreted in terms of a circumstellar disk with an inner hole, a scenario which is largely supported by both photometric (Sipos et al. 2009, Lorenzetti et al 2012a) and mainly interferometric (Akeson et al. 2005, Eisner et al. 2010) studies.

#### 4 Mid-IR variability

To ascertain if EXors present significant fluctuations in the *WISE* mid-IR range as they certainly do in the optical/near-IR, we have collected in Tables 2 and 3 the observations carried out in the L ( $\sim 3\mu\text{m}$ ), M ( $\sim 5\mu\text{m}$ ), N ( $\sim 10\mu\text{m}$ ), and Q ( $\sim 20\mu\text{m}$ ) bands and presented so far in the literature. To construct these Tables we have adopted the following data: all the ground-based observations, IRAS 12 and  $25\ \mu\text{m}$ , MSX 12 and  $21\ \mu\text{m}$ , *Spitzer* IRAC 3.4 and  $4.5\ \mu\text{m}$ , and *Spitzer* MIPS  $24\ \mu\text{m}$ . Data taken in different, although adjacent, bands (eg. IRAC 5.8 and  $8.0\ \mu\text{m}$ ) have not been considered because of the large difference between their and *WISE* band-passes. The epoch of any single observation and the effective wavelength of the used band-pass are also given in Tables 2 and 3. For an easier comparison, the values corresponding to the L, M (N, Q) bands are given in magnitudes (in Jansky): in some cases, the photometric values found in the literature have been converted into magnitude or fluxes by adopting the zero-magnitude fluxes given in the WEB resources of the Gemini Observatory (<http://www.gemini.edu/?q=node/11119>), whenever the conversion values are not given in the original paper. This procedure, together with the comparison between band-passes which are not perfectly coincident, is affected by instrumental and calibration effects and may cause a scatter that we conservatively estimate up to  $\pm 0.5\text{mag}$ . This scatter is much larger than the errors of any single measurement, nevertheless it has to be considered as the real uncertainty. Hence, fluctuations up to that amplitude have to be considered negligible for the present work, unless they have been

detected with the same instrumentation: in these latter cases the fluctuations are assumed to be significant if their amplitude is larger than the  $3\sigma$  uncertainty. IRAS fluxes are listed just for completeness, but not considered for the quantitative comparison, because they are taken with a beam size much larger than that of other observations. Data in Tables 2 and 3, complemented with *WISE* observations, are summarized in Figure 4, which shows a histogram of sources as a function of the amplitude of their fluctuations in the two most illustrative bands (L and N), for both classical (dashed black line) and newest (solid red line) EXors. Only the long-term (months, years) variations are considered here; the measurements dealing with fluctuations on a daily time-scale will be discussed below in this Section. We have computed (for any given source) the averaged values  $\overline{L}$  and  $\overline{F_N}$  of the L-band magnitude and N-band flux, respectively. Then,  $\Delta\text{mag}$  values have been computed for any single observation as  $|L - \overline{L}|$  and  $|2.5 \cdot \text{Log}(F_N/\overline{F_N})|$ . Therefore, for each source we have as many  $\Delta\text{mag}$  values as the available observations; in Figure 4 we depict the maximum value of the variability index  $I$ , defined as  $\Delta\text{mag}/0.5 \text{ mag}$  or  $\Delta\text{mag}/3\sigma$ , depending on how the observational set was obtained (i.e. different or same instrumentation, respectively).

As mentioned before, the fluctuations corresponding to the first bin are conservatively neglected; larger  $I$  values are mainly found for the newest objects: this fact is due in part to their intrinsically different nature (i.e. dominated by colder dust), but it is also a bias related to the larger number of mid-IR observations available for the newest sources. The amplitude of these fluctuations is comparable with that occurring in the near-IR, where a decreasing trend with increasing wavelength was noted (Lorenzetti et al. 2007). In other words, it seems that from  $\lambda > 2\text{-}3 \mu\text{m}$  the amplitude of the fluctuations becomes independent on  $\lambda$ . This likely means that the decreasing trend of  $\Delta\text{mag}$  in the optical and near-IR bands is essentially related to the stellar component only, while in the frequency regime where dust emission starts to dominate, any spectral trend is not that evident.

The time-scale of the mid-IR variability is even more important than the variability itself, since it can elucidate on the physical mechanism responsible for the fluctuations. The aforementioned analysis is typically based on time-scales of months, years or even longer, while only investigations at shorter time-scales can effectively constrain the working physical mechanism(s). To that scope, it is worthwhile to extract from Tables 2 and 3 the observations executed on shorter time-scales (days) and with the same instrumentation, so as to avoid uncertainties coming from possible inter-calibration issues. These cases are summarized in Table 4 where we list epoch and spectral band of the monitoring (cols.2 and 3), the number of observations available in that period (col.4), the parameter  $|x - \overline{x}|_{\text{max}}$  (col.5), which corresponds to the largest variation (with respect to the mean value) observed in that period, and the relative  $3\sigma$  uncertainty (col.6). This result is compatible with the *WISE*

multi-epoch data discussed in Sect.2: indication of short-time variability was given there for the source DR Tau, while V1180 Cas, and V512 Per did not present enough data to reach a firm conclusion.

These very short time-scales can be related to the response time of the dust particles to the energy input provided by the accretion event or, alternatively, to fast changes of the dust distributions (Kun et al. 2011). Basing upon a still rather poor statistics (3 positive cases out of 3 investigated), we can tentatively conclude that all EXors could be affected by variations of the same amplitude on the same time-scale (days): if this were the case, the response of the dust particle should be preferred to the dust re-arrangements, since the constancy of the observables seems more compatible with an intrinsic property of the dust grains, more than with a changing of the dust morphology, which should unexpectedly follow the same modalities. However, to ascertain the role of the two possible mechanisms, (quasi-)simultaneous ground-based observations in the near- and mid-IR (L, M bands) should be in order.

## 5 Concluding remarks

We have compiled the first collection of *WISE* photometry (3.4 - 22  $\mu\text{m}$ ) of the mid-IR emission of both classical and newest EXor objects. Analysing the presented data the following conclusions can be summarized:

- The *WISE* photometry along with the compilation of all the mid-observations retrieved from the literature represents the first step for constructing a mid-IR database of the EXor continuum emission.
- In the *WISE* two-color plots the classical and the newly defined EXors are distinguishable since the latter present a more prominent emission by their circumstellar disks, which appears also colder and less evolved.
- EXor SED's confirm the previous result providing piece of evidence in favour of the presence an inner hole in the circumstellar disk, as predicted by theory and observed by interferometric investigations.
- We began a search for mid-IR variability and preliminary results indicate that (i) the amplitude of the fluctuations is comparable to that occurring in near-IR without any decreasing trend with wavelength and that (ii) all the sources sampled on a daily time-scale present significant variations. Implications on possible mechanisms responsible for this behaviour have been discussed.



## 6 Acknowledgements

This publication makes use of data products from the Wide-field Infrared Survey Explorer, which is a joint project of the University of California, Los Angeles, and the Jet Propulsion Laboratory/California Institute of Technology, funded by the National Aeronautics and Space Administration. It makes also use of data products from the Two Micron All Sky Survey, which is a joint project of the University of Massachusetts and the Infrared Processing and Analysis Center/California Institute of Technology, funded by the National Aeronautics and Space Administration and the National Science Foundation.

## References

- Ábrahám, P., Kóspál, Á., Csizmadia, Sz., Moór, A., Kun, M., & Stringfellow, G. 2004, A&A, 419, L39
- Akeson, R.L. et al. 2005, ApJ, 622, 440
- Aspin, C. 2011a, AJ, 141, 196
- Aspin, C. 2011b, AJ, 142, 135
- Aspin, C. et al. 2009, ApJ, 692, L67
- Aspin, C., Beck, T.L., & Reipurth, B. 2008, AJ, 135, L35
- Aspin, C. & Sandell, G. 1994, A&A, 288, 803
- Aspin, C. & Sandell, G. 1997, MNRAS, 289, 1
- Appenzeller, I., Jankovics, I. & Krautter, J. 1983, A&A 53, 291
- Breger, M., Gehrz, R.D. & Hackwell, J.A. 1981, ApJ 248, 963
- Chen, X., Launhardt, R. & Henning, T. 2009, ApJ 691, 1729
- Cohen, M. 1974, MNRAS, 169, 257
- Cohen, M. & Kuhi, L. 1979, ApJS, 41, 743
- Cohen, M. & Schwartz, R.,D. 1983, ApJ, 265, 887
- Cutri, R.M. et al. 2012, <http://wise2.ipac.caltech.edu/docs/release/allsky/expsup/>
- D'Alessio, P., Calvet, N., Hartmann, L., Lizano, S. & Cantó, J. 1999, ApJ 527, 893
- Eisner, J.A. et al. 2005, ApJ, 718, 774
- Elias, J.H. 1978, ApJ, 224, 857
- Fischer, W.J. et al. 2012, arXiv:1207.2466v1
- Ghez, A.M., Emerson, J.P., Graham, J.M., Meixner, M. & Skinner, C.J. 1994, ApJ, 434, 707
- Glass, I.S. & Penston, M.V. 1974, MNRAS 167, 237
- Guieu, S. et al. 2009, ApJ, 697, 787
- Hartmann, L. et al. 2005, ApJ, 629, 881
- Hartmann, L., & Kenyon, S. 1985, ApJ, 299, 462
- Herbig, G.H. 1989, Proc. of the ESO Workshop on *Low Mass Star Formation and Pre-Main Sequence Objects*, ed. B. Reipurth, p.233

- Herbig, G.H. 2008, AJ, 135, 637
- Hernández, J. et al. 2007, 662, 1067
- Hodapp, K.-W., Hora, J.L., Rayner, J.T., Pickles, & Ladd, E.F. 1996, ApJ, 468, 861
- Hoffman, D.I., Cutri, R.M., Masci, F.J., Fowler, J.W., Marsh, K.A., & Jarrett, T.H. 2012, AJ, 143, 118
- Hughes, J., Hartigan, P., Krautter, J., & Kelemen, J. 1994, AJ, 108, 1071
- Kenyon, S.J. et al. 1994, AJ, 107, 2153
- Kenyon, S.J. & Gómez, M. 2001, AJ, 121, 2673
- Kóspál, Á., Ábrahám, P., Prusti, T., Acosta-Pulido, J., Hony, S., Moór, A., & Siebenmorgen, R. 2007, A&A, 470, 211
- Kóspál, Á. et al. 2012, ApJS, 201, 11
- Kun, M. et al. 2011, ApJ, 733, L8
- Liseau, R., Lorenzetti, D., & Molinari, S. 1992, A&A, 253, 119
- Lorenzetti, D. et al. 2012a, ApJ, 749:188
- Lorenzetti, D. et al. 2012b, Ap&SS, 343 Issue 2, 535
- Lorenzetti, D., Giannini, T., Larionov, V.M., Kopatskaya, E., Arkharov, A.A., De Luca, M., & Di Paola, A. 2007, ApJ, 665, 1182
- Lorenzetti, D., Larionov, V.M., Giannini, T., Arkharov, A.A., Antonucci, S., Nisini, B., & Di Paola, A. 2009, ApJ, 693, 1056
- McCabe, C., Ghez, A.M., Prato, L., Duchêne, G., Fisher, R.S., & Telesco, C. 2006, ApJ, 636, 932
- Muzerolle, J., Megeath, S.T., Flaherty, K.M., Gordon, K.D., Rieke, G.H., Young, E.T., & Lada, C.J. 2005, ApJ, 620, L107
- Persi, P., Tapia, M., Gómez, M., Whitney, B.A., Marenzi, A.M., & Roth, M. 2007, AJ, 133, 1690
- Przygodda, F., van Boekel, R., Ábrahám, P. et al. 2003, A&A 412, L43
- Rebull, L.M., Stauffer, J.R., Megeath, S.T., Hora, J.L., & Hartmann, L. 2006, ApJ, 646, 297
- Rieke, G.H., & Lebofsky, M.J. 1984, ApJ, 288, 618
- Rydgren, A.E. 1984, Publ. USNO, 25, 1
- Rydgren, A.E., Strom, S.E., & Strom, K.M. 1976, ApJS, 30, 307
- Rydgren, A.E. & Vrba, F.J. 1983, AJ 88, 1017
- Sipos, N. et al. 2009, A&A, 507, 881
- Stecklum, B., Melnikov, S.Y., & Meusinger, H. 2007, A&A, 175, 231
- Strutskie, M.F. et al. 2006, AJ, 131, 1163
- Thi, W.F. et al. 2001, ApJ, 561, 1074
- Weaver, W.B. & Jones, G. 1992, ApJS 78, 239
- Wright, E.L. et al. 2010, AJ, 140, 1868

Table 1  
WISE photometry of EXor objects.

Source	3.4 $\mu$ m	err 1	4.6 $\mu$ m	err 2	12 $\mu$ m	err 3	22 $\mu$ m	err 4	var.flag <sup>a</sup>	(2MASS)		$\varepsilon$
					(mag)					D (")	PA (deg)	
UZ Tau E	6.34	0.04	5.72	0.02	3.67	0.01	1.78	0.01	00nn	0.3	223.8	5.8
VY Tau	8.48	0.02	8.03	0.02	6.22	0.02	4.73	0.03	0019	0.1	150.3	1.7
DR Tau	5.68	0.06	4.67	0.04	2.99	0.01	1.04	0.02	0085	0.1	81.0	8.9
V1118 Ori	9.85	0.02	9.01	0.02	6.92	0.10	3.48	0.05	0019	0.1	150.3	9.7
NY Ori	6.87	0.03	6.27	0.02	3.30	0.02	0.93	0.03	009n	0.4	275.0	21.6
V1143 Ori	11.37	0.02	10.90	0.02	8.68	0.03	6.40	0.06	0011	0.2	111.0	1.8
EX Lup	8.19	0.02	7.63	0.02	4.50	0.01	2.33	0.02	1110	0.2	195.9	3.5
V1180 Cas	9.56	0.02	8.29	0.02	5.56	0.01	3.61	0.04	nnnn	0.18	258.4	534
V512 Per	6.75	0.03	4.89	0.03	1.44	0.01	-1.69	0.01	10nn	0.28	116.1	212
LDN1415 IRS	10.71	0.02	8.94	0.02	4.94	0.01	1.46	0.01	7941	4.6	5.8	1041
V2775 Ori	6.78	0.03	5.41	0.03	3.03	0.01	0.75	0.01	0019	0.10	23.2	5951
V1647 Ori	6.26	0.05	4.85	0.03	1.90	0.01	-0.48	0.01	0151	0.10	241.6	3233
GM Cha	10.07	0.03	7.79	0.02	4.24	0.01	0.91	0.01	1642	0.30	40.8	1706
OO Ser	11.83	0.03	8.94	0.02	4.47	0.01	0.59	0.01	0320	0.70	192.0	>1.3 10 <sup>4</sup>
V2492 Cyg	5.90	0.05	4.32	0.03	2.01	0.01	0.09	0.01	1097	—	—	5.5
V2493 Cyg	9.50	0.02	8.47	0.02	6.70	0.02	4.75	0.05	9999	2.53	196.0	14.9

- The fluxes corresponding to zero magnitude are: 309.5, 171.8, 31.67, and 8.363 Jy for the bands at 3.4, 4.6, 12, and 22  $\mu$ m, respectively (Cutri et al. 2012).
- The quality flag is AAAA for all sources.
- Saturation affects photometry for sources brighter than approximately 8.1, 6.7, 3.8, and -0.4 mag at 3.4, 4.6, 12, and 22  $\mu$ m, respectively.

<sup>a</sup> - *n* indicates insufficient or inadequate data to make a variability determination. Values of 0 through 5 can generally be regarded as non-variable sources in that band. Values of 6 and 7 can be regarded as potentially variable with small amplitudes. Objects with a value of 8 or 9 are most likely flux variables in the given band.

Table 2  
L and M band photometry of EXors.

Source	Epoch	L band		M band	
		(mag)	$[\lambda_{eff}]$ - Ref	(mag)	$[\lambda_{eff}]$ - Ref
UZ Tau E	73/74	$6.2 \pm 0.2$	[3.6] - 1		
	Nov 76	6.29	[3.4] - 2		
	Dec 76	$6.4 \pm 0.1$	[3.4] - 2	$5.6 \pm 0.3$	[4.8] - 2
	Nov 77	$6.04 \pm 0.02$	[3.5] - 3		
	Jan 81	6.29	[3.4] - 4	5.55	[4.8] - 4
	Dec 01 <sup>a</sup>	$6.42 \pm 0.17$	[3.5] - 5		
	Mar 04	$5.98 \pm 0.03$	IRAC[3.4] - 6	$5.46 \pm 0.04$	IRAC[4.5] - 6
VY Tau	73/74	$8.6 \pm 0.2$	[3.6] - 1		
	Dec 73	$8.3 \pm 0.1$	[3.5] - 7		
	Nov 77	$8.9 \pm 0.1$	[3.5] - 3		
	Dec 81	$8.50 \pm 0.06$	[3.5] - 8		
	Dec 01	$8.31 \pm 0.09$	[3.5] - 5		
DR Tau	72/74	$5.9 \pm 0.2$	[3.6] - 1		
	Nov 73	$5.8 \pm 0.05$	[3.5] - 7	$5.0 \pm 0.2$	[4.8] - 7
	Nov 77	$4.83 \pm 0.05$	[3.5] - 3		
	Dec 81	$5.34 \pm 0.04$	[3.5] - 8		
	Dec 81	$5.15 \pm 0.04$	[3.5] - 8	4.17	[4.8] - 4
	Nov 87	5.01 - 5.32	[3.8] - 9	4.47 - 4.69	[4.7] - 9
	Sep 88	4.93 - 5.46	[3.8] - 9		
	96/98	5.3 <sup>b</sup>	[3.4] - 10		
	Mar 04			4.5	IRAC[4.5] - 6
V1118 Ori	Oct 04	$9.85 \pm 0.002$	IRAC[3.4] - 11	$9.08 \pm 0.002$	IRAC[4.5] - 11
NY Ori	Sep 75	> 9	[3.6] - 12		
V1143 Ori					
EX Lup	Jun 73	> 8.7	[3.4] - 13		
	Apr 82	$8.02 \pm 0.01$	[3.8] - 14		
	Apr 82	$8.05 \pm 0.01$	[3.4] - 15	$7.54 \pm 0.05$	[4.8] - 15
	Feb/Sep 97	$(8.0-8.2) \pm 0.1$	[3.6] - 16		
	Mar 05	$7.92 \pm 0.02$	IRAC[3.4] - 16	$7.35 \pm 0.02$	IRAC[4.5] - 16

Table 2  
Continued.

Source	Epoch	L band		M band	
		(mag)	$[\lambda_{eff}]$ - Ref	(mag)	$[\lambda_{eff}]$ - Ref
V1180 Cas	Mar 09	9.50± 0.06	IRAC[3.4] - 17	8.58± 0.04	IRAC[4.5] - 17
	Oct/Nov 09	(8.99-9.28)±0.01	IRAC[3.4] - 17	(8.05-8.30)± 0.01	IRAC[4.5] - 17
V512 Per	< 83	6.37±0.01	[3.5] - 18	4.71±0.09	[4.6] - 18
	Sep 88	(5.20-5.59)±0.03	[3.91] - 19	> 4.2	[4.7] - 19
	Jan 89	(5.3-5.7)±0.2	[3.91] - 19	> 4.7	[4.7] - 19
	Feb 90	5.3±0.1	[3.91] - 19	> 4.4	[4.7] - 19
	Oct 90	5.28±0.02	[3.91] - 19	4.2±0.1	[4.7] - 19
	Sep 91	5.88±0.05	[3.6] - 20		
	Mar 92	6.11±0.05	[3.6] - 20		
	Nov 92	6.11±0.05	[3.42] - 20		
	Feb 93	5.96±0.05	[3.42] - 20		
	Oct 93	6.27±0.05	[3.42] - 20		
	Dec 93	6.48±0.05	[3.42] - 20		
	Dec 93	6.60±0.05	[3.42] - 21		
	Sep 04	7.45±0.07	IRAC[3.4] - 22	6.39±0.09	IRAC[4.5] - 22
LDN1415IRS					
V2775 Ori	Feb/Oct 04	8.46±0.05	IRAC[3.4] - 23	7.66±0.05	IRAC[4.5] - 23
V1647 Ori	Mar 04	5.33	IRAC[3.4] - 24	4.41	IRAC[4.5] - 24
	Feb 07	7.6±0.1	[3.4] - 25		
	Sep 08	5.8±0.1	[3.4] - 25		
	Feb 11	5.6±0.1	[3.4] - 25		
GM Cha	Mar 99	8.32±0.05	[3.5] - 26		
	Jul 04	8.42±0.08	IRAC[3.4] - 27	6.98±0.07	IRAC[4.5] - 27
OO Ser	Oct 95	6.9	[3.8] - 28	5.2	[4.8] - 28
	Feb 96	8.1±0.1	[3.6] - 29	5.36±0.01	[4.8] - 29
	Apr 96	8.2±0.1	[3.6] - 29	5.45±0.03	[4.8] - 29
	Sep 96	8.22±0.08	[3.6] - 29	5.84±0.04	[4.8] - 29
	Oct 96	8.9±0.4	[3.6] - 29	5.9±0.4	[4.8] - 29
	Mar 97	8.9±0.1	[3.6] - 29	6.13±0.05	[4.8] - 29
	Apr 97	9.06±0.08	[3.6] - 29	5.98±0.04	[4.8] - 29
	Sep 97			6.3±0.4	[4.8] - 29
	Apr 04	11.5±0.1	IRAC[3.4] - 29	8.35±0.02	IRAC[4.5] - 29
V2492 Cyg	Jul 06	8.94±0.09	IRAC[3.4] - 30	7.6±0.1	IRAC[4.5] - 30
	Sep 10	5.4±0.1	[3.8] - 30		
	Nov 10	6.0±0.1	[3.8] - 30		
V2493 Cyg	Nov 77	9.4±0.1	[3.5] - 3		
	Aug 06	9.9±0.1	IRAC[3.4] - 31	9.2±0.1	IRAC[4.5] - 31

- References to the Table: (1) Cohen 1974; (2) Elias 1978; (3) Cohen & Kuhl 1979; (4) Rydgren 1984; (5) McCabe 2006; (6) Hartmann et al. 2005; (7) Rydgren et al. 1976; (8) Rydgren & Vrba 1983; (9) Kenyon et al. 1994; (10) Thi et al. 2001; (11) Rebull et al. 2006; (12) Breger et al. 1981; (13) Glass & Penston 1974; (14) Appenzeller et al. 1983; (15) Hughes et al. 1994; (16) Sipos et al. 2009; (17) Kun et al. 2011; (18) Cohen & Schwartz 1983; (19) Liseau et al. 1992; (20) Aspin & Sandell 1994; (21) Aspin & Sandell 1997; (22) Chen et al. 2009; (23) Fischer et al. 2012; (24) Muzerolle et al. 2005; (25) Aspin 2011b; (26) Kenyon & Gómez 2001; (27) Persi et al. 2007; (28) Hodapp et al. 1996; (29) Kóspál et al. 2007; (30) Aspin 2011a; (31) Guieu et al. 2009.

<sup>a</sup> This value refers to the total binary system, although the primary and the secondary have been resolved and separately observed.

<sup>b</sup> ISO-SWS continuum flux near H<sub>2</sub> lines.

Table 3  
N and Q band photometry of EXors.

Source	Epoch	N band		Q band	
		(Jy)	$[\lambda_{eff}]$ - Ref	(Jy)	$[\lambda_{eff}]$ - Ref
UZ Tau E	73/74	$1.6 \pm 0.3$	[10] - 1		
	Nov 76	$1.3 \pm 0.3$	[10] - 2		
	Dec 76	$1.0 \pm 0.2$	[10] - 2		
	Jan 81	$1.1 \pm 0.1$	[10] - 3	0.8	[20] - 3
	83	$1.38 \pm 0.03$	IRAS[12]- 4	$1.76 \pm 0.04$	IRAS[25] - 4
	Dec 92 <sup>a</sup>	$1.06 \pm 0.04$	[9.5] - 5		
	Nov 99 <sup>b</sup>	$1.5 \pm 0.1$	[10.8] - 6	$1.6 \pm 0.2$	[18.1] - 6
VY Tau	73/74	$< 0.35$	[10] - 1		
	Dec 73	$0.3 \pm 0.05$	[10.8] - 7		
	83	$0.20 \pm 0.03$	IRAS[12]- 4	$0.29 \pm 0.03$	IRAS[25] - 4
	Nov 99	$0.07 \pm 0.01$	[10.8] - 6		
DR Tau	72/74	2.2	[10] - 1		
	Nov 73	1.3	[11.1] - 7		
	83	$3.16 \pm 0.03$	IRAS[12]- 4	$4.30 \pm 0.05$	IRAS[25] - 4
	96/98	2.4 <sup>c</sup>	[9.6] - 8		
	Dec 81	3.8	[10] - 3	2.9	[20] - 3
	Dec 82	2.9	[10] - 3		
	96/98	2.4 <sup>c</sup>	[9.6] - 9		
	Dec 02	2.0	[11.9] - 10		
V1118 Ori	Jan 02	$< 0.5$	MSX[12] - 11		
	Jan 06	$0.07 \pm 0.01$	[10.4] - 11		
NY Ori	83	$10 \pm 3$	IRAS[12]- 4		
V1143 Ori	83	$0.17 \pm 0.04$	IRAS[12]- 4	$0.10 \pm 0.06$	IRAS[25] - 4
EX Lup	83	$0.80 \pm 0.03$	IRAS[12]- 4	$1.09 \pm 0.03$	IRAS[25] - 4
	Feb/Sep 97	$(0.7-0.8) \pm 0.1$	ISOPHOT[12]- 12	$(0.9-1.3) \pm 0.2$	ISOPHOT[20] - 12

Table 3  
Continued.

Source	Epoch	N band		Q band	
		(Jy)	$[\lambda_{eff}]$ - Ref	(Jy)	$[\lambda_{eff}]$ - Ref
V1180 Cas	83	< 0.25	IRAS[12]- 13	0.72 FQUAL 3	IRAS[25] - 13
V512 Per	< 83	6.54±0.07	[10.2] - 14	25±1	[19] - 14
	83	11.2 FQUAL3	IRAS[12] - 13	42.8 FQUAL 3	IRAS[25] - 13
	Sep 04			> 21 (satur.)	MIPS[24] - 15
LDN1415IRS	83	0.15±0.05	IRAS[12]- 16	0.49±0.06	IRAS[25] - 16
V2775 Ori	Apr 05			0.68±0.03	MIPS[24] - 17
	Nov 08			5.0±0.2	MIPS[24] - 17
V1647 Ori	83	0.52	IRAS[12]- 18	1.2	IRAS[25] - 18
	Mar 04	7±1	[11.2] - 19	15.6	MIPS[24] - 20
	Mar 07	0.23	[11.2] - 21	0.44	[18.3] - 21
	Sep 08	2.8±0.5	[11.2] - 19	7±1	[18.3] - 19
GM Cha	Apr 04	1.15±0.09	[12.9] - 22		
OO Ser	Oct 95	6.4	[11.7] - 23	12.5	[20.6] - 23
	Feb 96	4±1	[12] - 24	29±3	[25] - 24
	Apr 96	4.1±0.1	[12] - 24	39±1	[25] - 24
	Sep 96	3±1	[12] - 24		
	Oct 96	4±1	[12] - 24	21±2	[25] - 24
	Mar 97	2.98±0.06	[12] - 24	18±2	[25] - 24
	Apr 97	3±1	[12] - 24	19±2	[25] - 24
	Sep 97	2.0±0.8	[12] - 24	17±2	[25] - 24
	Apr 04			13±2	MIPS[24] - 24
	Oct 04	0.6±0.1	[10.4] - 24		
V2492 Cyg	83	3.4±0.3	IRAS[12] - 25	6.6±0.6	IRAS[25] - 25
	Jul 96	2.5±0.1	MSX[12.13] - 25	3.1±0.2	MSX[21.4] - 25
	Jul 06			3.4±0.3	MIPS[24] - 25
V2493 Cyg					

- References to the Table: (1) Cohen 1974; (2) Elias 1978; (3) Rydgren et al. 1984; (4) Weaver & Jones 1992 (5) Ghez et al. 1994; (6) McCabe 2006; (7) Rydgren et al. 1976; (8) Thi et al. 2001; (9) Thi et al. 2001; (10) Przygodda et al. 2003; (11) Lorenzetti et al. 2007; (12) Sipos et al. 2009; (13) IRAS Point Source Catalog; (14) Cohen & Schwartz 1983; (15) Chen et al. 2009; (16) Stecklum et al 2007; (17) Fischer et al. 2012; (18) Ábrahám et al. 2004; (19) Aspin et al. 2009; (20) Muzerolle et al. 2005; (21) Aspin et al. 2008; (22) Persi et al. 2007; (23) Hodapp et al. 1996; (24) Kóspál et al. 2007; (25) Aspin 2011a;

<sup>a</sup> Spectrophotometry of the resolved component UZ Tau E in the 8-13  $\mu$ m window: observations at close-by wavelengths are also available.

<sup>b</sup> These values refer to the total binary system, although the primary and the secondary have been resolved and separately observed.

<sup>c</sup> ISO-SWS continuum flux near H<sub>2</sub> lines.

Table 4

Short time-scale (days) mid-IR monitoring cases of a few EXors.

Source	Epoch	Band	$N_{obs}$	$ x - \bar{x} _{max}$	$3\sigma$
(mag)					
DR Tau	Nov 87	L	13	0.16	0.03
	Sep 88 <sup>a</sup>	L	33	0.28	0.03
V1180 Cas	Oct/Nov 09	L	12	0.17	0.03
	Oct/Nov 09	M	12	0.14	0.03
V512 Per	Sep 88	L	7	0.20	0.09

<sup>a</sup> This sampling was obtained also on hours time-scale.



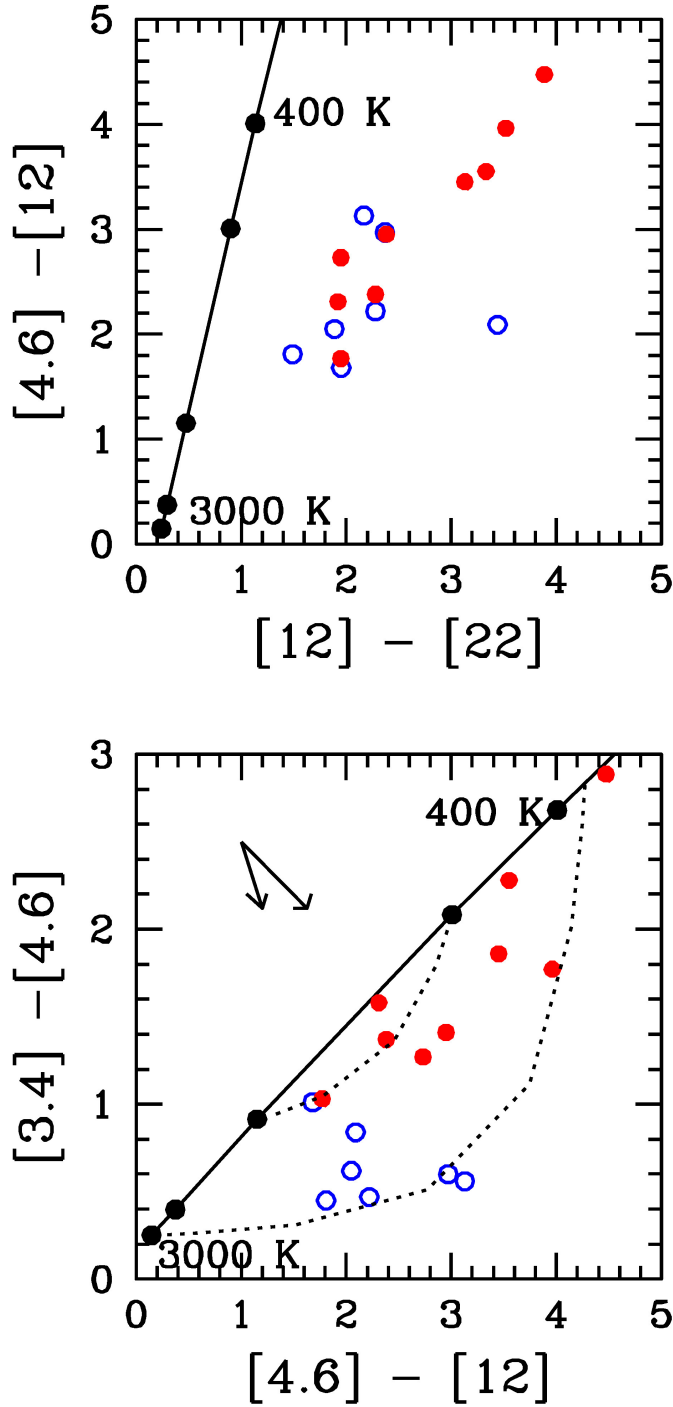


Fig. 1. *WISE* two color diagrams of EXOrs. The colors of the classical (newest) EXOrs are depicted with blue (red) open (solid) symbols. The size of the error bars is typically comparable to the size of the points. The black-body colors (at different temperatures) are indicated by the black straight line, with the solid circle marks corresponding to a temperature of 400, 500, 1000, 2000, and 3000 K, from right to left). The black dashed lines in the lower panel indicate the colors of the sum of two black-bodies, where the surface of coldest one (in the range 380-500 K) is progressively increased with respect to that of the warmest (in the range 1000-3000 K). The reddening vectors correspond to an extinction  $A_V = 10$  mag and were computed from Rieke & Lebofsky (1985); two different values for the  $12\mu\text{m}$  extinction were assumed: equal to  $A_\lambda$  at  $10.5\mu\text{m}$  in Rieke & Lebofsky table (leftmost vector) and equal to  $A_\lambda$  at  $12.0\mu\text{m}$ .

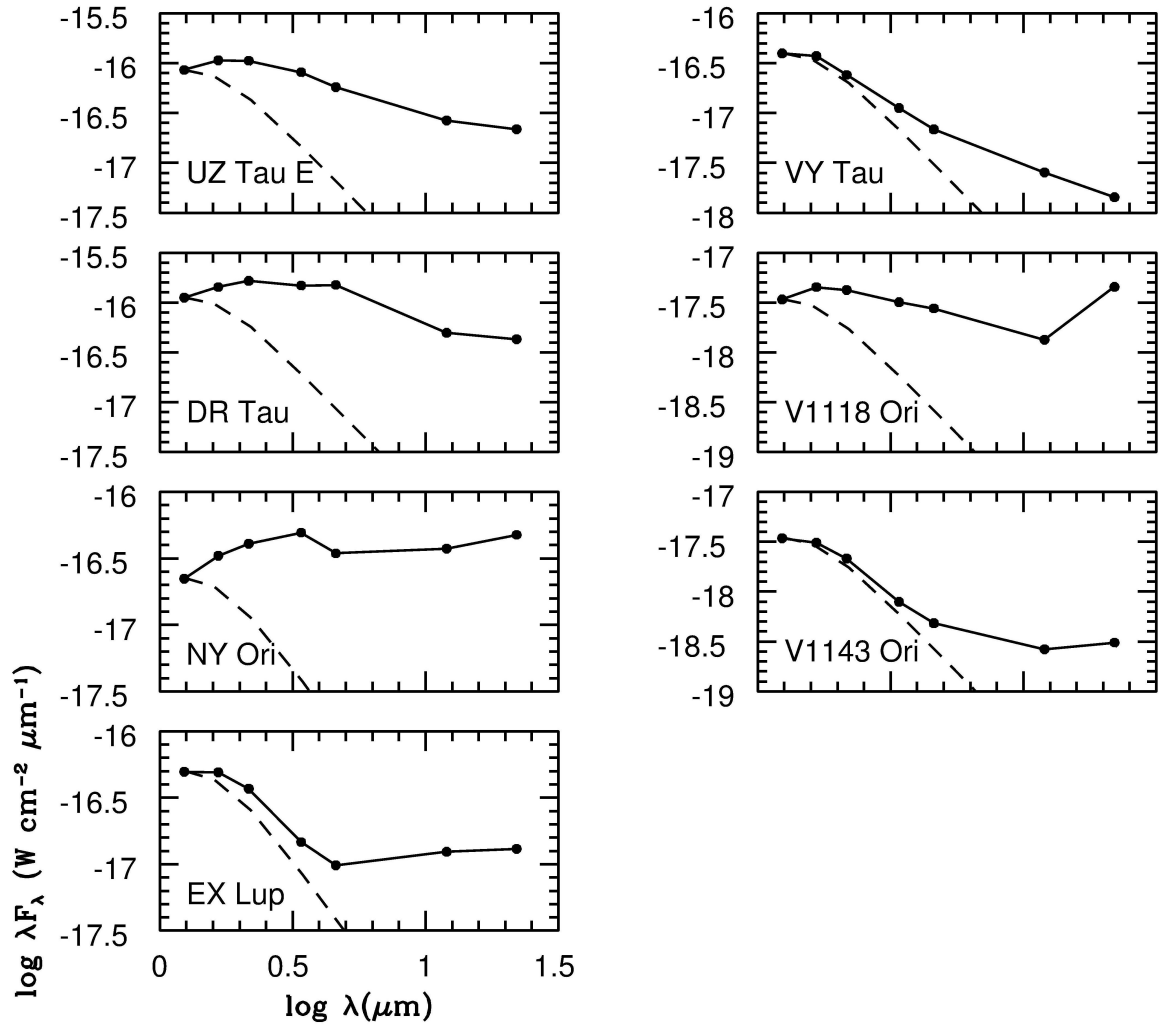


Fig. 2. SED's of the *classical* EXor sources in the range 1.25-22  $\mu\text{m}$ , composed by 2MASS and *WISE* fluxes. Dashed line represents a median photosphere of stars in the spectral type range K5-M5 and normalized to the J-band flux of the source.

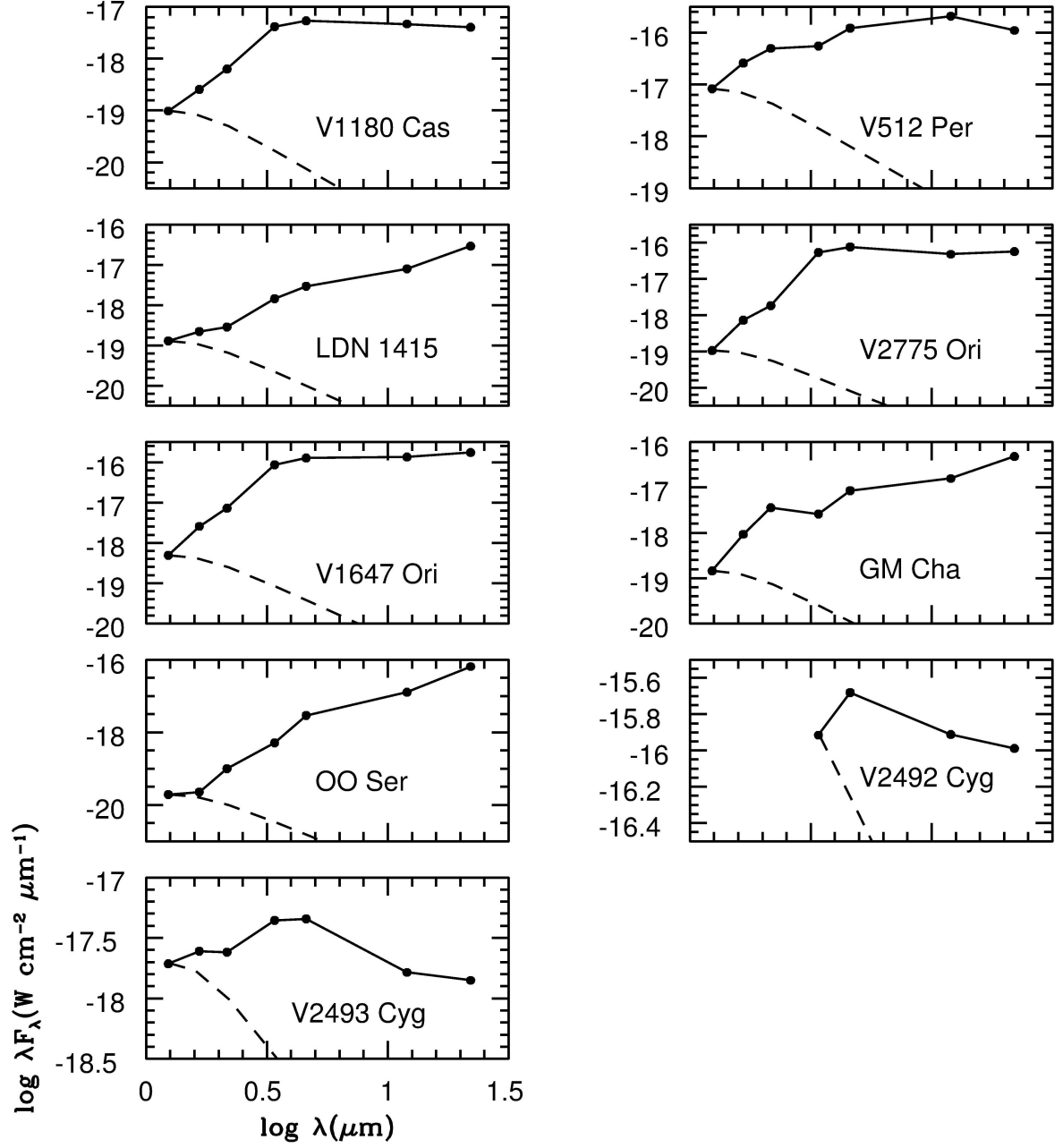


Fig. 3. Same as Figure 2 for the *newest* EXor sources.

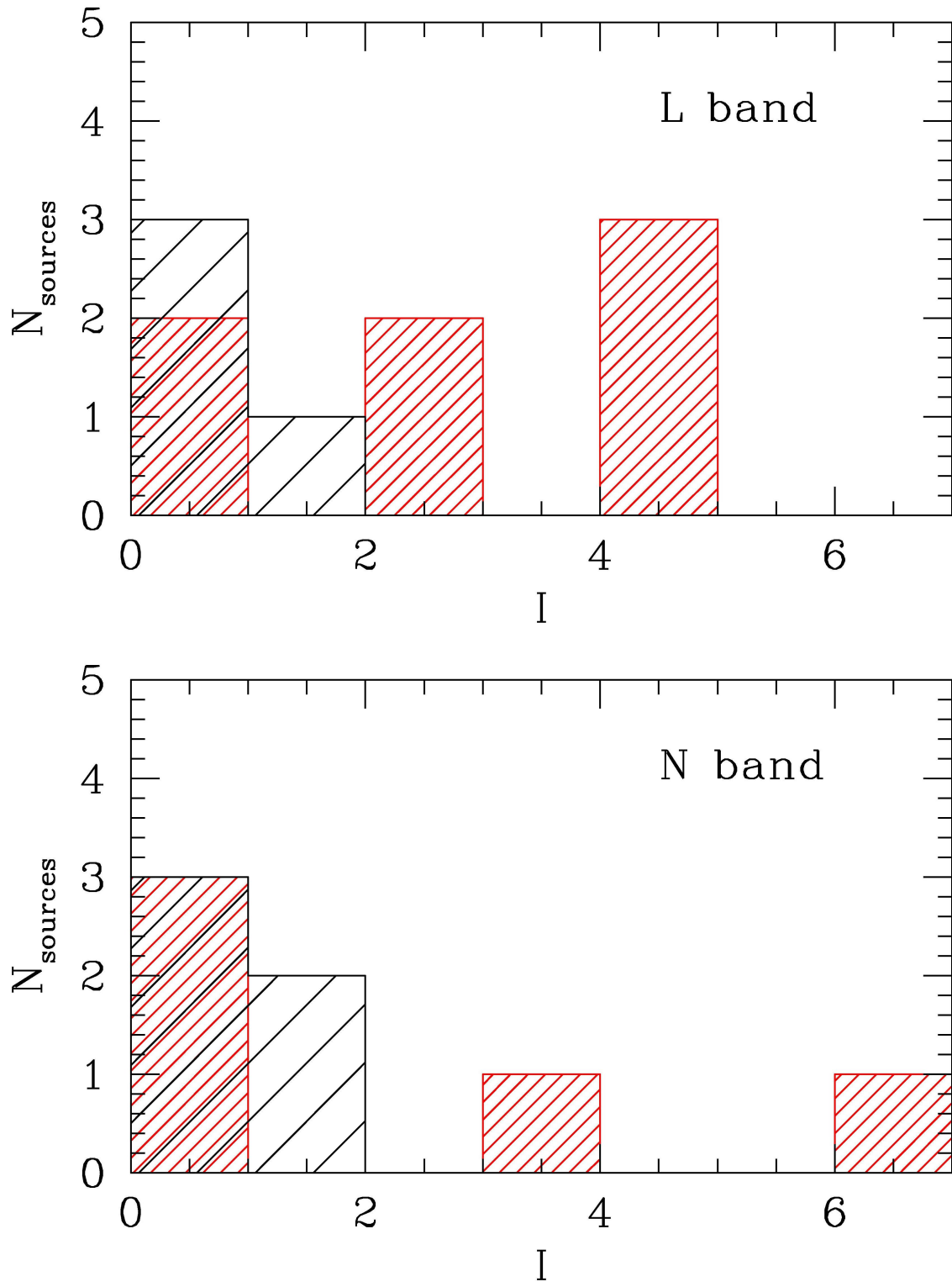


Fig. 4. Distribution of the EXor fluctuations expressed in terms of the variability index  $I$  (see text) in the L and N bands (see Tables 2 and 3).